

GT2011-45713

A validation of commercial flow solver performance on hybridised octree meshes

WP Kellar & SA Harvey
Cambridge Flow Solutions Ltd,
Compass House, Vision Park, Cambridge, CB4 9AD,
UK
and
WN Dawes,
CFD Laboratory, Department of Engineering,
University of Cambridge, Cambridge, CB2 1PZ

Abstract

In recent years we have been developing a meshing system which is aimed at eliminating the bottleneck represented by building meshes for real-world, complex turbomachinery configurations. This system is based on a rapid octree meshing technology which is then made conformal to the bodies present. The objective of this paper is to demonstrate that this class of mesh is not only very fast to produce but also fit-for-purpose in the sense that simulations generated with third-party commercial flow solvers like Fluent have the same accuracy as those performed on more conventional meshes. A range of standard examples and test cases will be presented.

Introduction

Mesh generation is a key pacing item in CFD and simulation in general and has been the subject of substantial research over many years. Several strands have emerged: structured multi-block, chimera, overset, fully unstructured and cut-Cartesian octree based meshes. A recent summary of this diversity can be found in Shontz [1]. Generally, the orthodoxy has been body-fitted meshes matched to explicit BREP geometry models (typically NURBS patches, edges and their associated bindings) but application to real-world, complex geometries remains a challenge and a bottleneck. However, a few publications, like Bussoletti et al [2] and Aftosmis et al [3], have shown the potential advantages of cut-Cartesian, octree

meshes in dealing with complex geometries – but the difficulty of managing the cut cells in the flow solver has been a barrier to widespread adoption. Combining this approach with a body-conformal paradigm holds out much promise as a way forward.

A series of papers, Dawes et al [4-9], describes work aimed at developing a mesh generator which can reliably produce meshes for geometries of essentially arbitrary complexity in an automated manner and fast enough to keep up with the pace of an engineering development program. Our goal is to be able to script the mesh generation within an automated workflow - and forget it.

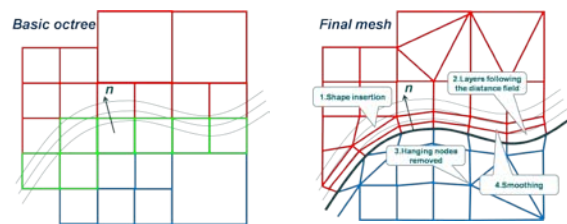


Fig.1: Body-conformal mesh generation via shape insertion and mesh morphing

This system is based on a rapid octree meshing technology which is then made conformal to the bodies present by a combination of shape insertion (mesh topology) and morphing (mesh optimisation) – together with the addition of near-wall layer mesh and interface-conjugate zones (see sketch in Figure 1). Natural

attributes of this class of meshing are, for example: 1:8 cell-volume transitions consequent on the inherent nature of an octree (albeit subsequently hybridised, polyhedralised and/or smoothed); localised mesh quality of the same class everywhere, independent of overall geometry complexity; and high-quality hex-dominant off-body mesh, with possibilities for relatively straightforward flow-based mesh adaption.

With our approach, complex geometries can be reliably converted into meshes containing many millions of cells in a matter of tens of minutes on a modest cpu cluster. This geometry can be "dirty" in the sense that there can be small gaps in the *stl* or the *stl* may be locally folded or distorted - our approach simply meshes over the top of these imperfections. Although the meshing can be driven by a GUI we have specifically designed the system to be fully automatable and scriptable to be embedded within a workflow. Figure 2 shows a mesh for a cooled blade.

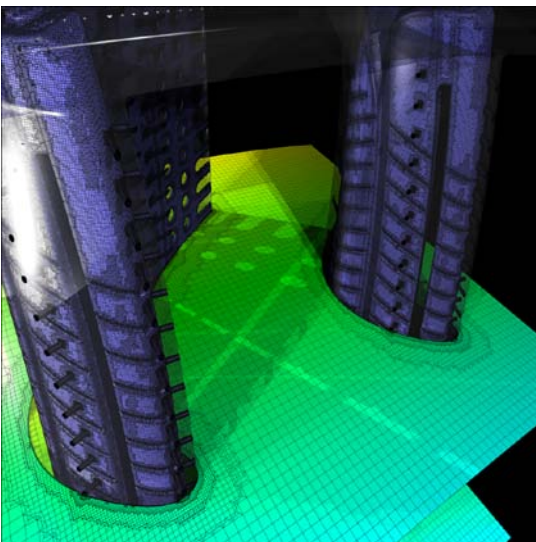
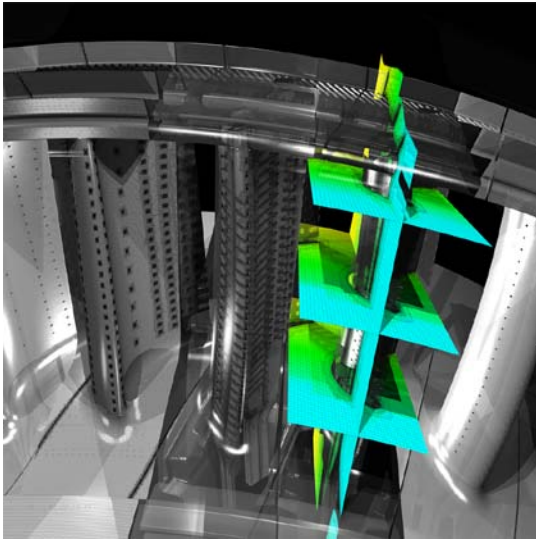


Fig.2: Mesh for a cooled turbine blade generated from manufacturing CAD exported as *stl*

However, the purpose of mesh generation is actually flow simulation, and the usefulness of any mesh and/or pre-processing approach can only be measured in terms of the quality of flow solution it enables.

The objective of this paper is to demonstrate that this class of body-conformal octree mesh (generated with our particular *Boxer* system as example) is not only very fast to produce, but also fit-for-purpose in the sense that simulations generated with third-party commercial flow solvers like Fluent have the same accuracy as those performed on more conventional meshes. A range of standard examples and test cases will be presented.

Test cases

Five test cases were selected as shown in Table 1 with their associated primary references. The first three are rather simple: an airfoil, a wing and a turbine blade. We have selected them as paradoxically they are more challenging for a mesh system such as ours in competition with an orthodox C- or O-mesh approach. The later cases introduce modest geometric complexity. We do not have access to any public domain experimental data for a geometry as complex as that shown in Figure 2.

1	RAE2822 airfoil	Cook et al [10]
2	ONERA M6 wing	Schmitt et al [11]
3	VKI turbine blade	Arts et al [12]
4	Rotating ribbed channel	Rigby [13]
5	Cut-back TE	Martini et al [14]

Table 1: The test cases and primary references

In the following Sections each test case will be addressed in turn.

Case 1: RAE2822

This transonic airfoil, Cook et al [10], has become a classic test case – both surface pressure and skin friction distributions are available. The test profile is shown in Figure 3.

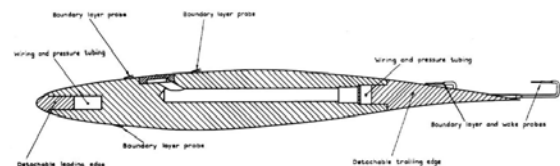


Fig.3: RAE2822 test profile

The key parameters used in the test selected are summarized in Table 2 below. We generated a mesh using *Boxer* resolving the flow down to $Y^+ \leq 5$ and extended sufficiently far from the airfoil. This mesh had ~0.9M cells in 3D (we cannot generate pure 2D meshes) containing the equivalent of around 250k cells

in 2D section. A near-view and detail view of the mesh is shown in Figure 4; note the near-wall layer mesh.

M_∞	0.73
α	2.8°
Re	6.5 million

Table 2: Key parameters for the RAE2822 airfoil

Simulations were performed using the well-known, industry-standard, flow solver Fluent run in second order accurate, density-based mode and with a standard $k-\omega$ turbulence model. The predicted results are compared with the experimental data in Figure 5. The pressure coefficient match is very satisfactory; the skin friction is predicted a little high but satisfactorily.

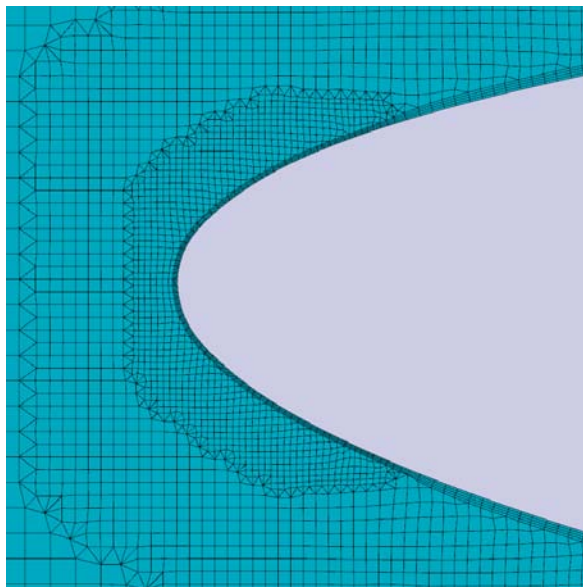
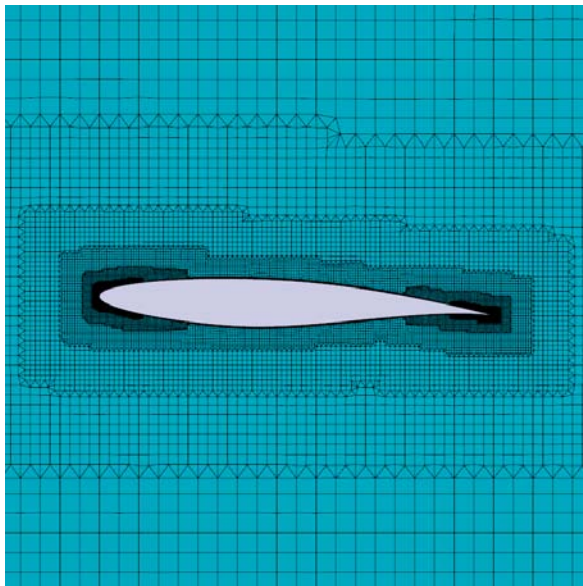


Fig.4: Near-view and detail view of the Boxer mesh generated for the RAE2822 test case.

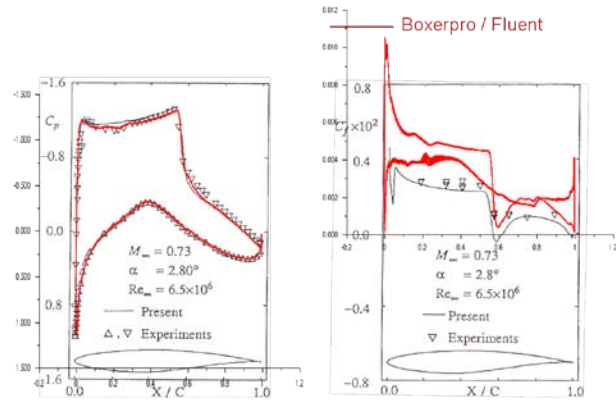


Fig.5: Predicted airfoil static pressure and skin friction distribution compared with experiment (“present”=CFD from Cook et al [10]).

Case 2: ONERA M6 wing

This classic test case, the ONERA M6 swept transonic wing (Schmitt et al [11]) was chosen for similar motives to the previous case: to demonstrate that our meshing system can support acceptable accuracy for very simple geometries which can already be easily meshed using conventional O- or C-mesh systems. The key aerodynamic parameters are shown in Table 2 below.

M_∞	0.8395
α	3.06°
Re	11.7 million

Table 2: Key parameters for the ONERA M6 swept wing case

A mesh containing ~9.5M cells was generated with $Y^+ \leq 5$ and very similar in form and character to that for the RAE2822 (see Figure 4) and so not repeated here for brevity. In this swept wing case neither the leading edge nor trailing edges of our mesh are axis-aligned providing a good test of the fidelity of the body-conformal mesh export from our octree-based meshing system.

Simulations were again performed using Fluent run in second order accurate, density-based mode and with a standard $k-\omega$ turbulence model. The predicted surface pressure distributions are compared in Figure 6 with both the experimental data and predictions made using the WIND flow solver (as reported in Schmitt et al [11]). The agreement of the current predictions with the other two data sets is very satisfactory with similar levels of agreement at each of the seven spanwise stations. Of particular note in this case is the resolution of the three-dimensional double shock structure over the central portion of the span.

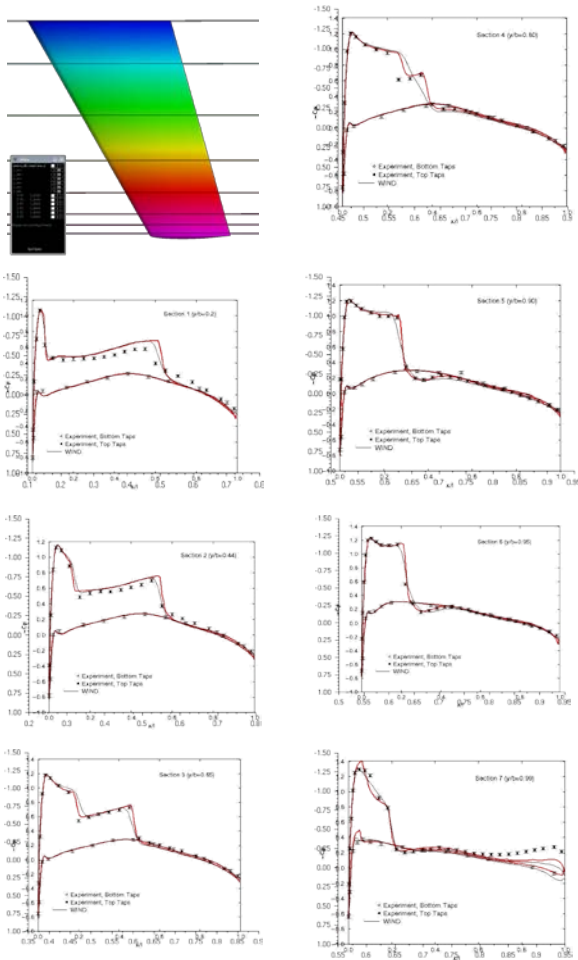


Fig.6: Predicted (red line=Boxer/Fluent, black line=WIND) vs measured distributions of pressure coefficient at seven spanwise locations on the ONERA M6 wing

Case 3: VKI transonic turbine blade

The next case is also a standard test case, this time a transonic turbine blade tested in cascade at the VKI and reported by Arts et al [12]. The key parameters are noted below in Table 3.

α_1	+48.4°
α_2	~ -68°
M_{2is}	1.12
Re	1.05 million
Turbulence at inlet	4%

Table 3: Key parameters for the VKI transonic turbine case

We generated a mesh using *Boxer* and resolving the flow down to $Y^+ \leq 2$ and extended sufficiently far up- and downstream from the blade. This mesh had ~0.9M

cells in 3D (we cannot generate pure 2D meshes) containing the equivalent of around 450k cells in 2D section. Mesh overviews and leading & trailing edge detail views are shown in Figures 7a-c. Of note are the near-wall layer mesh and the solution adapted mesh in the region of the blade wake.

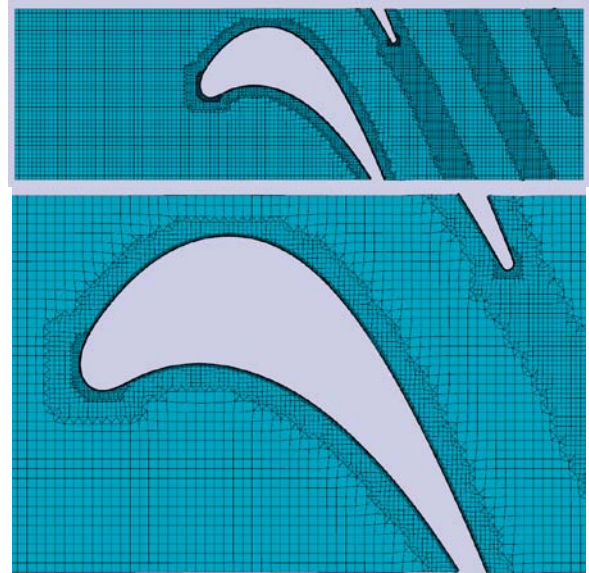


Fig.7a: Mesh overviews for the VKI turbine

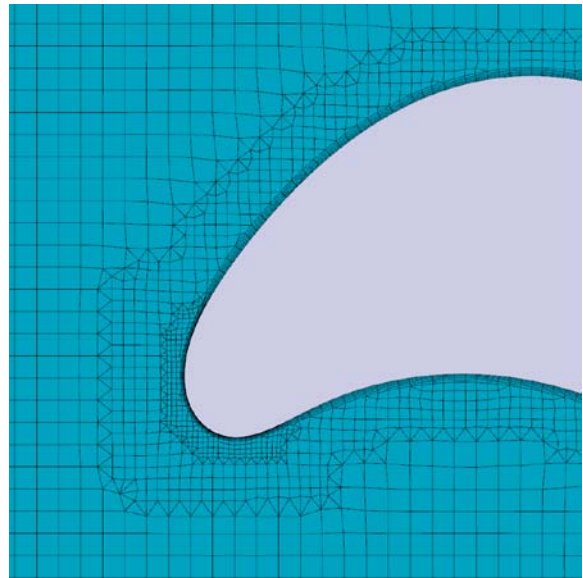


Fig.7b: Mesh detail – leading edge

Simulations were performed using Fluent run in second order accurate, density-based mode but this time using a realizable $k-\epsilon$ (with non-equilibrium wall function). Figure 8 shows a comparison of measured blade surface isentropic Mach numbers and heat transfer coefficient with predictions from the present Boxer/Fluent simulations and those obtained from CANARI and reported in Arts et al [12]. For isentropic Mach number the level of agreement is very good; for

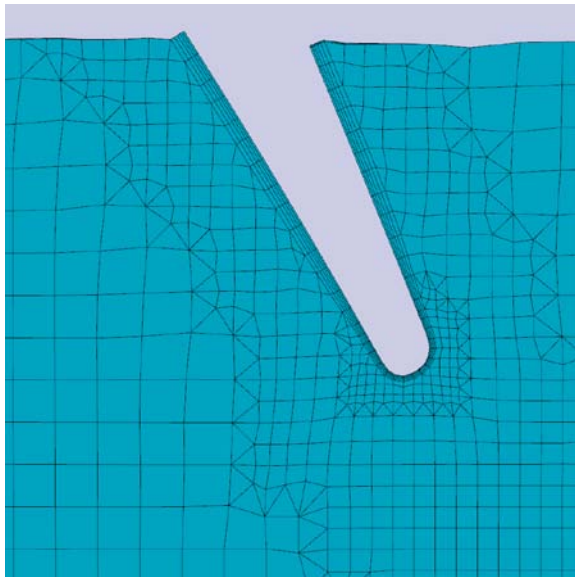


Fig. 7c: Mesh detail – trailing edge (before adaptive mesh refinement for the wake)

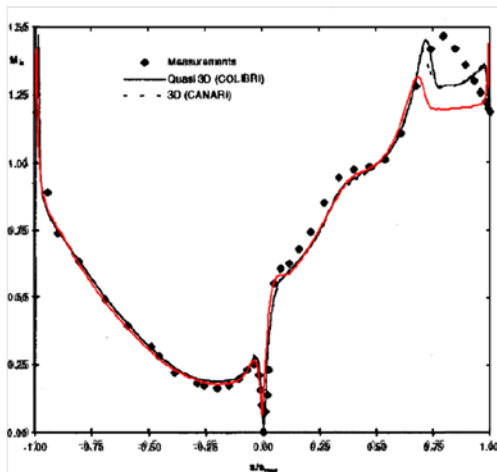


Fig. 10 Computed velocity distributions ($\theta = -5$ deg, $M_{2,le} = 1.092$)

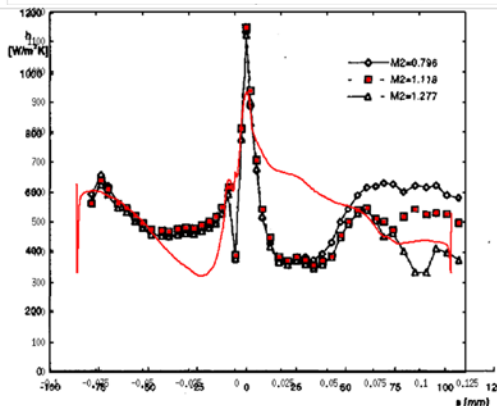


Fig. 6 Measured heat transfer distributions: influence of $M_{2,le}$ ($\theta = -5$ deg, $Tu_{\infty} = 4$ percent, $Re_{2,le} = 1.05 \times 10^6$)

Fig.8: Predicted (red line=Boxer/Fluent, black line=CANARI) vs measured distributions of isentropic Mach number & heat transfer coefficient

heat transfer coefficient, the agreement is less good on the suction side and certainly would benefit from a transition model being used in the simulations. There are no grounds to suspect mesh quality to be responsible for the discrepancy.

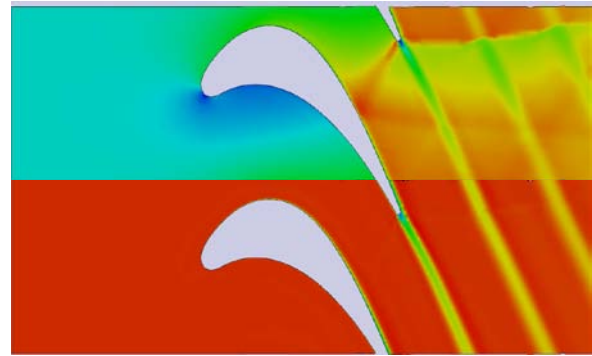


Fig.9: Mach number (range 0. to 1.4), top, and total pressure p_0/p_{01} (range 0.325 to 1.04), bottom

Finally the “off-body” resolution is shown in Figure 9 via field plots of Mach number and total pressure ratio. The shock system and the wakes, supported on the adapted mesh, are crisply resolved and satisfactory.

Case 4: Rotating ribbed channel

The next case is a rotating ribbed channel reported by Rigby [13]. Figure 10 shows a schematic of the geometry and Table 4 the key parameters.

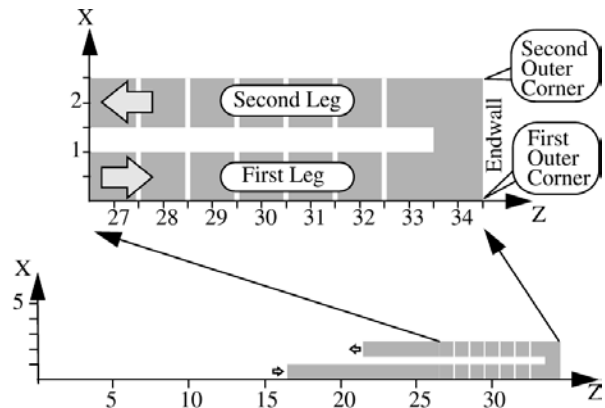


Fig. 1. Schematic of geometry

Fig.10: Schematic of geometry (Rigby [12])

Rotation # Ro	0.24
Re	5500
rpm	753
Wall/inlet T ratio	1.2
Mass flow (kg/s)	0.0016

Table 4: Key parameters for the rotating ribbed channel case

A relatively fine mesh was generated using *Boxer* and is shown in Figure 11; the ribs were well resolved and wall layers used. The range of Y^+ was 1-5.

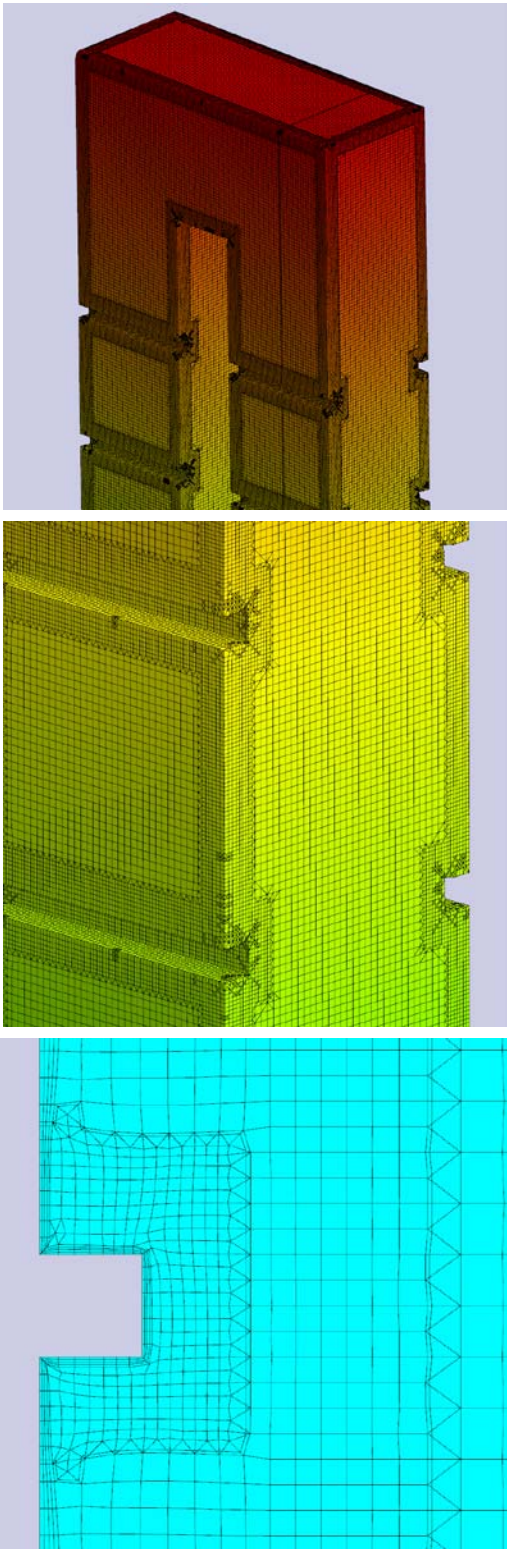


Fig.11: Selected mesh views for the rotating ribbed channel case

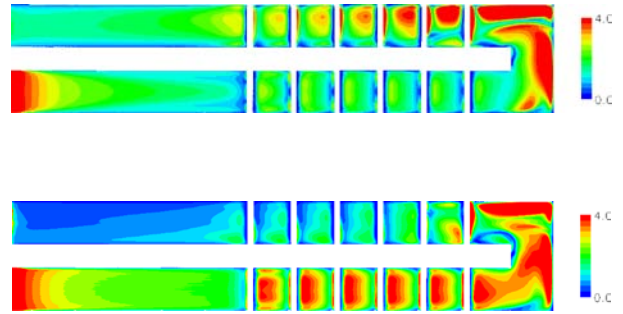


Fig.12: Contours of Nu/Nu_0 with range 0 to 4; top – leading channel; bottom – trailing channel.

Simulations were performed using Fluent run in second order accurate, density-based mode and using a realizable $k-\epsilon$ (with non-equilibrium wall function).

Results are presented in terms of a normalised Nusselt number defined as:

$$Nu/Nu_0 = (hD/k) / 0.23 Re^{0.8} Pr^{0.4}$$

where $h = Q/(T_{wall} - T_{ref})$ with the reference temperature T_{ref} taken as a linear function between inlet and outlet.

Figure 12 shows contours of Nu/Nu_0 for the leading surface of the channel and the trailing. The highly three dimensional nature of the flow is clear – particularly in terms of the secondary flow structures in the 180° bend.

Figures 13 and 14 show a comparison of predicted and measure spanwise averaged heat transfer coefficient in the first and in the second leg of the rotating channel.

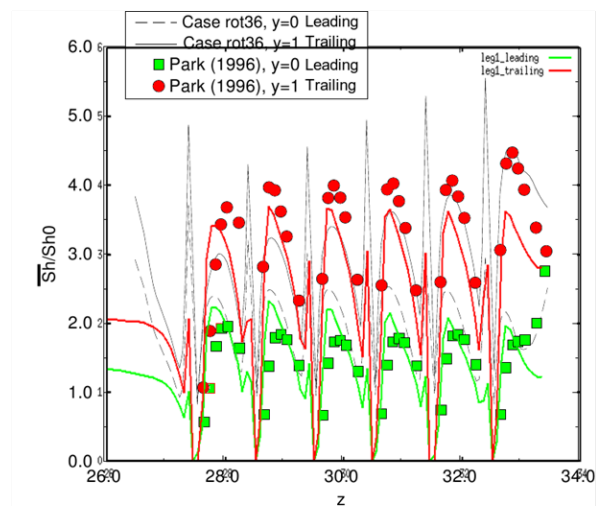


Fig. 16. Spanwise averaged Sherwood number in the first leg

Fig.13: Predicted (line) and measured (symbol) spanwise averaged heat transfer coefficient in the first leg of the channel (green=leading, red=trailing)

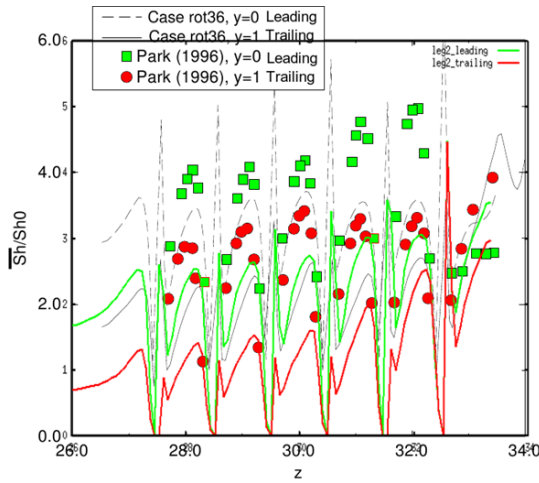


Fig. 17. Spanwise averaged Sherwood number in the second leg

Fig.14: Predicted (line) and measured (symbol) spanwise averaged heat transfer coefficient in the second leg (green=leading, red=trailing)

The agreement is generally good in the first leg but rather less so in the second leg due to difficulty in modeling the physics of the secondary flow structures in the 180° bend rather than due to mesh quality or resolution.

Case 5: Cut-back trailing edge

Finally we consider a cut-back trailing edge test case published by Martini & Schultz [14] and arising from an EU FP6 Programme of research into turbine cooling called AITEB. An overview of the geometry is given in Figure 15 showing the test configuration and the CAD model used to generate the mesh.

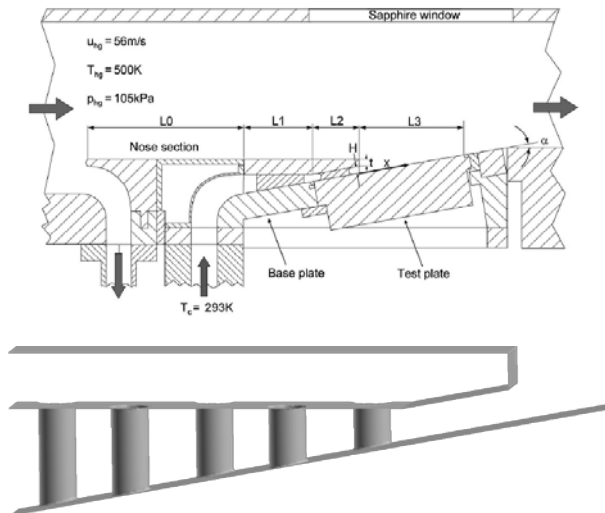


Fig.15: Overview of the cut-back trailing edge geometry: top, the test configuration; bottom the CAD model used to generate the mesh

Table 5 shows the key parameters. All surfaces are adiabatic except for the test-plate on the lower wall which has either zero or fixed heat flux accordingly.

Free stream Mach #	0.125
Re	250,000
Free stream Tu	7%
Free stream T ₀	500K
Coolant T ₀	295K
Density ratio	1.5

Table 5: Key parameters for the cut-back trailing edge test case

Two meshes were generated using *Boxer* containing 1M and 6M cells and similar to the mesh shown below in Figure 20.

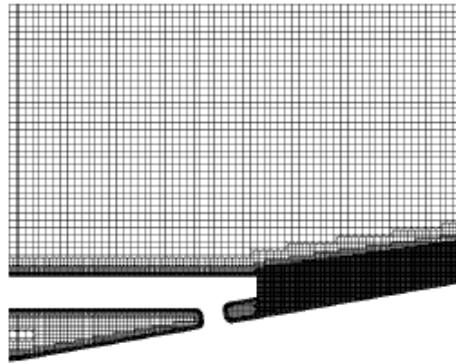


Fig.16: Section cut through the cut-back trailing edge mesh.

Simulations were performed using Fluent run in second order accurate, density-based mode and using a realizable k-ε (with non-equilibrium wall function).

Results, on the coarser 1M cell mesh and for two blowing ratios, are shown in Figures 17 and 18. Figure 17 shows the predicted spatial distribution of film cooling effectiveness on the test-plate. Figure 18 compares the laterally averaged film cooling effectiveness with the measurements of Martini & Schultz [14]; the agreement is rather poor.

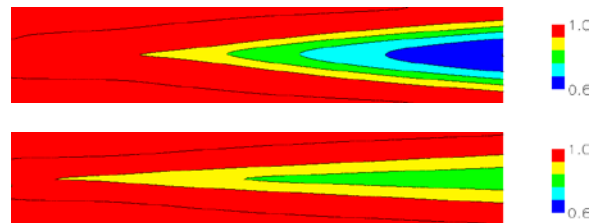


Fig.17: Predicted spatial distribution of film cooling effectiveness plotted vs. X/L: top, blowing ratio of 0.5; bottom 1.10

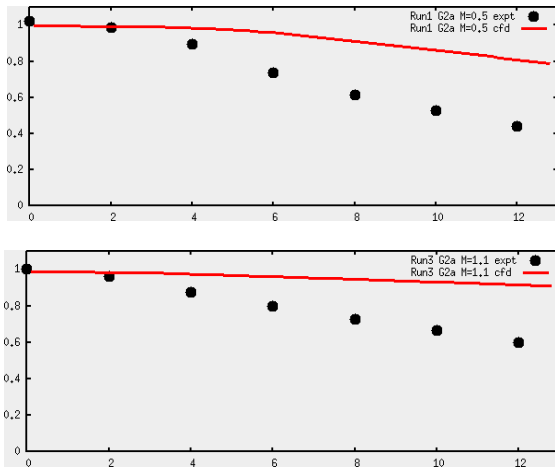


Fig.18: Laterally averaged film cooling effectiveness plotted vs. X/L: top, blowing ratio of 0.5, bottom 1.10

Re-running the case with 6M cells instead of 1M made very little difference as can be seen from Figure 19.

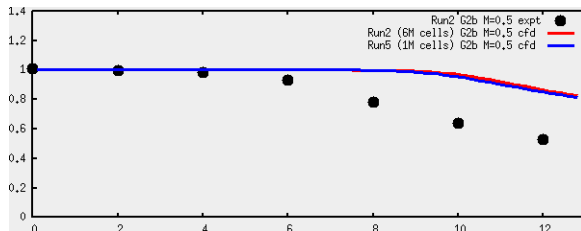


Fig.19: Mesh refinement study for the case with blowing ratio 0.5: 1M & 6M cells

This poor level of agreement between steady RANS simulations and measurement was also noted by Martini et al [14]. Figure 20 shows some of their simulations with CFX Tascflow (using $k-\omega$) on a structured multi-block mesh.

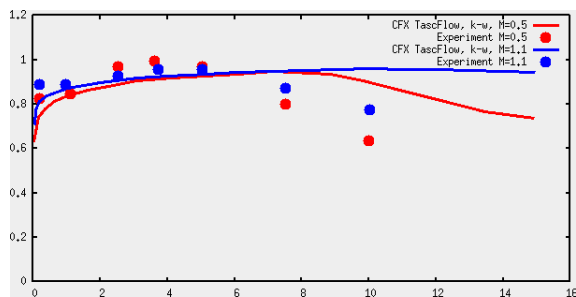


Fig.20: Comparison of measured and predicted laterally averaged film cooling effectiveness values for blowing rates M=0.5 and 1.1 (Martini et al [14])

As Martini et al [14] noted the most likely explanation for this systematic discrepancy is that the real flow is unsteady (driven by the instability of the shear layer) and simply not capable of being modeled by any steady RANS turbulence model. Accordingly they performed

LES simulations and the time averaged data was in very much better agreement with measurement.

To perform LES simulations is beyond the scope of this paper but a relevant question is whether our particular mesh type is LES-friendly in terms of mesh quality. LES was successfully performed by Tucker et al [15] on a similar geometric configuration with the mesh shown in Figure 16; Figure 21 reproduces the instantaneous temperature field and associated streamlines – the large scale unsteadiness is apparent.

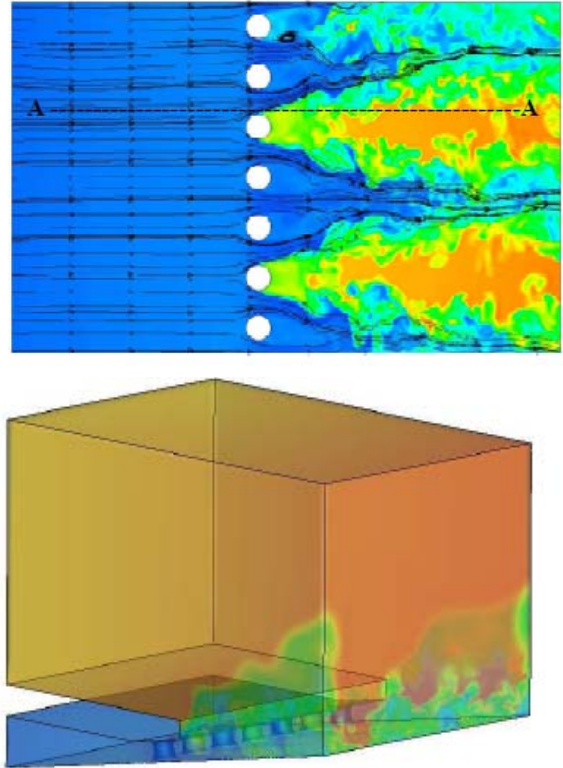


Fig.21: Instantaneous temperature field & streamlines (Tucker et al [15])

Concluding Remarks

Hybridized octree meshes of the class produced by our Boxer software are extremely quick to produce, tolerant of dirty geometry and capable of automatically handling very complex geometries.

The objective of this paper was to show that this class of mesh is also perfectly capable of supporting good quality flow simulations using a commoditized, commercial, off-the-shelf code. This objective has been achieved and demonstrated via a series of public domain test cases. Where there were discrepancies between measurement and simulation this was consistent with well-known and often reported deficiencies in the physical modeling deployed – not due to the meshing itself.

Acknowledgements

We would like to thank the support of our Development Partners for the encouragement and funding for this work.

References

[1] Shontz S, Editor, Proceedings of the 19th International Meshing Roundtable, Chattanooga TN, 2010

[2] Bussioletti JE, Johnson FT, Bieterman MB, Hilmes CL, Melvin RG, Young DP & Drela M "TRANAIR: solution-adaptive CFD modelling for complex 3D configurations" AIAA Paper 1995-0451, 1985

[3] Aftosmis MJ, Berger MJ & Melton JE, "Robust and efficient Cartesian mesh generation for component-based geometry" AIAA J., 36, 6, 952-, 1999

[4] Dawes WN "Building Blocks Towards VR-Based Flow Sculpting" " 43rd AIAA Aerospace Sciences Meeting & Exhibit, 10-13 January 2005, Reno, NV, AIAA-2005-1156

[5] Dawes WN, Kellar WP, Harvey SA "Towards a fully integrated parallel geometry kernel, mesh generator, flow solver & post-processor" 44th AIAA Aerospace Sciences Meeting & Exhibit, 9-12 January 2006, Reno, NV, AIAA-2006-45023

[6] Dawes WN, Kellar WP, Harvey SA "Viscous Layer Meshes from Level Sets on Cartesian Meshes" 45th AIAA Aerospace Sciences Meeting & Exhibit, 8-11 January 2007, Reno, NV, AIAA-2007-0555

[7] Dawes WN, Kellar WP, Harvey SA "Towards topology-free optimisation: an application to turbine internal cooling geometries" 46th AIAA Aerospace Sciences Meeting & Exhibit, 7-10 January 2008, Reno, NV, AIAA-2008-925

[8] Dawes WN, Kellar WP, Harvey SA "A practical demonstration of scalable parallel mesh generation" 47th AIAA Aerospace Sciences Meeting & Exhibit, 9-12 January 2009, Orlando, FL, AIAA-2009-0981

[9] Dawes WN, Kellar WP, Harvey SA "Generation of conjugate meshes for complex geometries for coupled multi-physics simulations" 87th AIAA Aerospace Sciences Meeting & Exhibit, 7-10 January 2010, Orlando, FL, AIAA-2010-062

[10] Cook PH, McDonald MA & Firmin MCP "Aerofoil RAE 2822 - Pressure Distributions, and Boundary Layer and Wake Measurements," *Experimental Data Base for Computer Program Assessment*, AGARD Report AR 138, 1979.

[11] Schmitt V & Charpin F "Pressure Distributions on the ONERA-M6-Wing at Transonic Mach Numbers," *Experimental Data Base for Computer Program Assessment*. Report of the Fluid Dynamics Panel Working Group 04, AGARD AR 138, May 1979.

[12] Arts T, Duboue JM & Rollin G "Aerothermal performance measurement and analysis of a two dimensional, high turning rotor blade" *Trans ASME, Journal of Turbomachinery*

[13] Rigby DL "Prediction of heat and mass transfer in a rotating ribbed coolant passage with a 180 degree turn" NASA TM-1999-208501

[14] Martini P, Schultz A & Bauer H-J "Film cooling effectiveness and heat transfer on the trailing edge cutback of gas turbine airfoils with various internal cooling designs" *Transactions of the ASME, Vol.128*, pp.196-, Jan. 2006

[15] Tucker P, Eastwood S, Klostermeier C, Xia H, Ray P, Tyacke J & Dawes WN "Hybrid LES approach for practical turbomachinery flows: Part 2 – further applications" ASME Paper GT2010-23807, Glasgow, June 2010

-oOo-